Available online at www.sciencedirect.com
SCIENCE DIRECT®
Scripta Materialia 53 (2005) 87–92
Scripta MATERIALIA
www.actamat-journals.com

Time-resolved strain mapping measurements of individual Portevin–Le Chatelier deformation bands

Wei Tong [a,*], Hong Tao [a], Nian Zhang [a], Louis G. Hector Jr. [b]

[a] *Department of Mechanical Engineering, Becton Engineering Center, Yale University, 219, Becton Center, 15, Prospect Street, New Haven, CT 06520-8284, USA*
[b] *Materials and Processes Lab, General Motor R&D Center, Warrant, MI 48090-9055, USA*

Received 29 September 2004; received in revised form 6 March 2005; accepted 9 March 2005
Available online 8 April 2005

Abstract

A technique based on high-speed digital photography and image correlation for direct whole-field strain mapping of Portevin–Le Chatelier deformation bands is described. Results for a type B band show that the deformation band was formed within a few milliseconds and remained stationary as no motion of the band was detected.

Keywords: Dynamic strain aging; Portevin–Le Chatelier effect; Tension test; Aluminum alloys; Image correlation strain mapping

1. Introduction

Unstable plastic flow in terms of nucleation of deformation bands associated with repeated serrated yielding are often observed macroscopically in metal alloys due to strong dynamic strain aging or the so-called Portevin–Le Chatetlier (PLC) effect [1–8]. The serrations are due to sudden strain bursts that are generally believed to result from interactions between moving dislocations and diffusing solute clouds, although other processes may also be involved [9]. The PLC effect is commonly observed in many aluminum alloys [10] and a variety of other materials [9,11–13]. However, it has been most extensively studied in the dilute solid solution Al–Mg alloys under uniaxial tension [2,3,8,10,11,14].

Progress has been made toward a general understanding of the microscopic-scale features underlying the PLC effect, and several mechanistic models have been proposed [15,16]. However, a complete understanding of the detailed micromechanical mechanisms that underlie macroscopic deformation behavior of serrated plastic flow is still lacking [4]. Of particular importance is PLC band nucleation, which has not been adequately quantified even at the macroscopic level [5–7,17,18]. Several nucleation and development mechanisms were conjectured by Chihab et al. [3] who used analog video technology and light contrast variation of polished surfaces due to PLC band formation to capture PLC band kinetics in an Al–Mg alloy tensile coupon. They concluded, however, that the slow video framing rate (25 fps, where fps = frames per second) in their experiments was inadequate and should be replaced with "fast cinematography" to more fully capture band nucleation and growth kinetics.

In the present study, we combine state-of-the-art high-speed digital photography with an experimental strain mapping measurement technique via image correlation [17–21] to both temporally and spatially characterize serrated plastic flow in an Al–Mg alloy in tension. We present here a first report on time-resolved direct strain mapping measurements to provide some insight into the nucleation and growth of individual PLC

* Corresponding author. Tel.: +1 203 432 4260; fax: +1 203 432 6775.
E-mail address: wei.tong@yale.edu (W. Tong).

1359-6462/$ - see front matter © 2005 Published by Elsevier Ltd. on behalf of Acta Materialia Inc.
doi:10.1016/j.scriptamat.2005.03.020

bands. In addition, we explore the issue of band propagation across the tensile coupon surface during the image capture times afforded by the high-speed camera.

2. Experimental procedure

An aluminum AA 5052-H32 sheet with alloying elements of 2.5 wt% Mg, 0.25 wt% Cr, and 0.1% Mn [22] was tested in the as-received condition in this study. The aluminum polycrystalline sheet was strain-hardened and stabilized at the H32 temper and was not strongly textured. It had a thickness of 0.95 mm and an average grain size of about 12 μm. To facilitate the image-based strain measurement of PLC bands at a sufficiently high spatial resolution, a tension test coupon with a 4.6 mm-wide gage section and 20 mm gage length was used, see Fig. 1(a). The test coupon was fully clamped at the both ends and stretched under displacement control by a screw-driven mini-tensile tester at a constant crosshead speed to achieve a nominal strain rate of $10^{-4}\ s^{-1}$. The mini-tensile tester, which is shown in Fig. 1(b), had overall dimensions of 100 mm by 125 mm by 50 mm, a total crosshead travel of 50 mm, and a load cell of 4.4 kN maximum capacity. Both force and displacement data were recorded digitally at a rate of 8 Hz. The uncertainty in the load measurement was ±0.3 N for the 4.4 kN miniature load cell. Tests were also carried out using a data acquisition rate of 100–250 Hz but with higher electronic noises.

Prior to the test, one flat surface of the tension test coupon was decorated with finely sprayed black paint speckles to enhance image contrast. To characterize the nucleation and growth of individual PLC bands during tensile testing, both temporally and spatially, the entire gage section of the test coupon was imaged with a high-speed digital camera using a special CMOS sensor operating at various framing rates ranging from 1000 to 5000 fps [23]. The high-speed camera was post-triggered when a sudden load drop associated with a single serration event was detected and a total amount of 8285 image frames prior to the triggering point were captured in the camera memory (see Fig. 2(a)). The tensile test was then interrupted (but without complete unloading) in order to download the images to a host computer

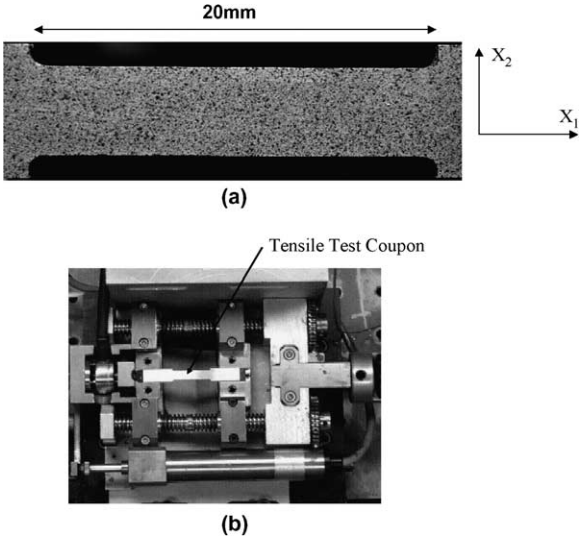

Fig. 1. (a) A digital image of the AA5052-H32 sheet metal tension coupon. Its surface was sprayed with black paint speckles and its gauge section is 20 mm long, 4.6 mm wide and 0.95 mm thick; (b) the screw-driven mini-tensile tester. The coordinate system X_1–X_2 used in the paper is also shown.

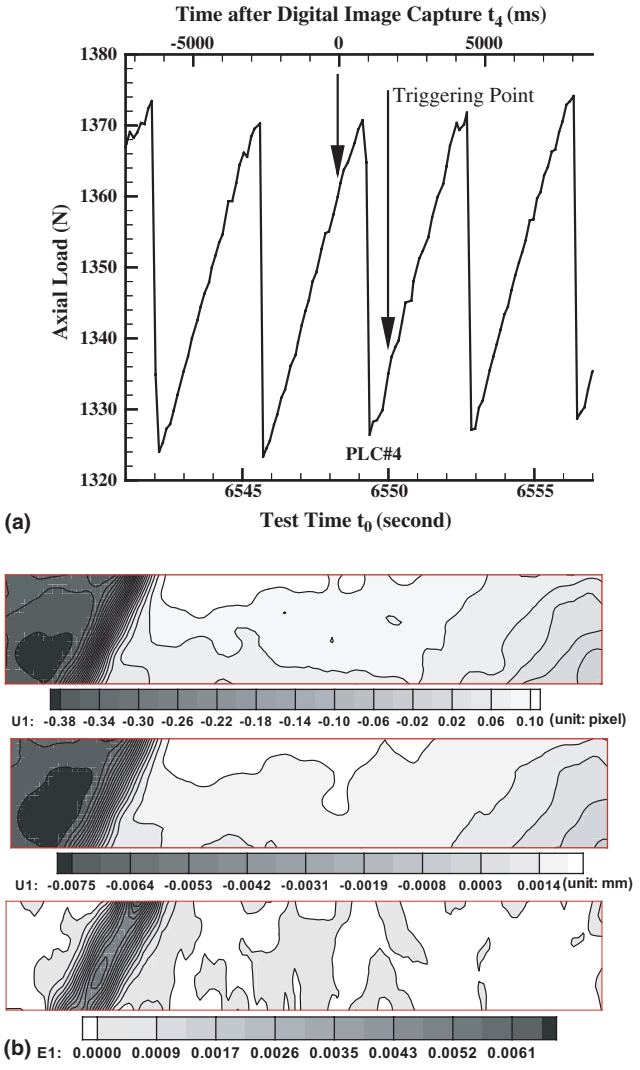

Fig. 2. (a) The force–time record of the tension test with arrow markers indicating the start (the first image frame) and end (the post-triggering point) of the image capture of PLC band #4; (b) the accumulated plastic deformation in terms of horizontal displacement U_1 (in both pixels and mm) and the axial strain E_1 contour map showing strain localization in band #4 over the image capture duration of 1.6568 s. The field of view of the contour maps is 22 mm by 4.6 mm of the tensile coupon surface as shown in Fig. 1(a).

via a high-speed Ethernet connection. More than 10 PLC band nucleation and growth events were imaged in our experiment. Each of the recorded 8-bit grayscale digital images had a size of 1344×280 pixels with a spatial resolution of 20.0 μm per pixel. The aspect ratio of the digital images was chosen to match closely that of the gage section of the tension coupon to maximize both the spatial and time resolution of the high-speed imaging acquisition. The recorded digital images were analyzed with the SDMAP [24] digital image correlation software that computes both cumulative and incremental surface strain maps of the test coupon surface for each image capture. Details behind the strain mapping via the digital image correlation analysis may be found in [19,21,24]. The axial strain reported here was computed locally using a bi-quadratic surface fitting of displacements over subsets of 40×40 to 60×60 pixels [19]. The errors in local in-plane displacements, rigid body rotation, and strain measurements were estimated to be 0.02 pixels, 0.02° and 100×10^{-6}, respectively, for a macroscopically homogenous field.

3. Results

Serrated plastic flow was detected in the AA5052-H32 tension coupon in Fig. 1(a) after an incubation plastic strain of about 1% when it was stretched at a nominal strain rate of $10^{-4}\,s^{-1}$ at the ambient temperature of 24 °C. Load drops with a magnitude of 30–40 N (corresponding to 7–9 MPa in stress or 2–4% of the current flow strength of the material) occurred rather regularly within a period of 4–5 s. Each load drop was associated with the nucleation and growth of a spatially discrete PLC band followed by a predominantly elastic reloading phase.

Out of more than 10 PLC bands captured by the high-speed digital photography, we selected one representative PLC band (#4) for a detailed description of digital image correlation analysis results. A total of 8285 digital image frames were continuously recorded with a time interval of 0.2 ms per frame for a total duration of 1.6568 s for the band. Fig. 2(a) and (b) show the experimental force–time records and whole-field strain mapping data. In Fig. 2(a), the serration time with its origin defined by the start of the image capture is given in the top horizontal axis in milliseconds as t_4. Note that the left arrow in the figure coincides with the load and time at the start of the image capture, while the right arrow designates the load and time at which recording was stopped (as the camera was post-triggered at this point). The time at which the load reached its local minimum (which coincided more or less with complete band formation) is labeled PLC #4. Fig. 2(b) shows the corresponding cumulative plastic deformation maps in terms of both horizontal displacement U_1 (top map in units of pixels, and middle map in mm) and true axial strain, E_1. These deformation maps were obtained via correlation analysis of frame 1 ($t_4 = 0$ s) and frame 8285 ($t_4 = 1.6568$ s) for the band. The densely spaced displacement contour lines denote the location, width, and orientation (about 26° clockwise from the transverse direction) of the PLC band. The symmetry in displacement conditions tended to favor alternating bands ±26° so that the relative vertical displacement at the grip ends was nearly zero on average. The axial strain contour map (bottom) details the distribution and magnitude of deformation inside the PLC band. Across the PLC band, there was a jump of about 0.45 pixel or 9 μm in horizontal displacement over an axial distance of about 150 pixels or 3 mm. The peak axial strain in PLC band #4 was about 0.6%.

Fig. 3(a) and (b) shows cumulative and incremental strain maps and the corresponding several selected times on their force–time curves associated with the nucleation and growth of PLC band #4. Each of the four cumulative strain maps in Fig. 3(a) was generated through digital image correlation of the very first image ($t_4 = 0$ s) with the image recorded at the indicated time. The time label in each map designates the capture time, which is referenced to the time at which the first image was captured at the outset of the capture event (denoted by the left arrows in Fig. 2(a)). The top left contour map in Fig. 2(a) (representing a capture time of 969.4 ms for band #4) shows the cumulative axial strain field just prior to a sudden load drop or the sudden nucleation and rapid growth of the band. It suggests that there was some precursory strain up to 0.1% that accumulated locally at one of the free edges of the tensile coupon before the sudden load drop. The second and third cumulative axial maps in Fig. 3(a) (representing capture times of 972.2 and 975.0 ms, respectively) show the development of the PLC bands during the sudden load drop. The last cumulative axial map in Fig. 3(a) (representing a capture time of 1656.8 ms) show fully formed PLC after some elastic reloading (i.e. along the increasing portion of the load curve) but prior to the nucleation of another PLC band.

Changes in strain contours associated with the PLC bands are shown very clearly by the incremental axial strain maps in Fig. 3(b). The incremental maps were generated through digital image correlation of two successive image frames captured at a 0.4 ms time interval. The time shown on each incremental axial strain map is the average of the capture times for these two image frames. The four incremental axial strain maps shown in Fig. 3(b) span a period of 1.6 ms or about 1/3 of the entire dynamic plastic deformation process during the formation of PLC bands #4. By dividing the axial strain increments with the time interval of 0.4 ms, the actual strain rate inside a PLC band $\dot{\varepsilon}_B$ was estimated to between 0.5 and $1\,s^{-1}$ and is much higher than the imposed overall strain rate $\dot{\varepsilon}_a$ of $10^{-4}\,s^{-1}$. However, the

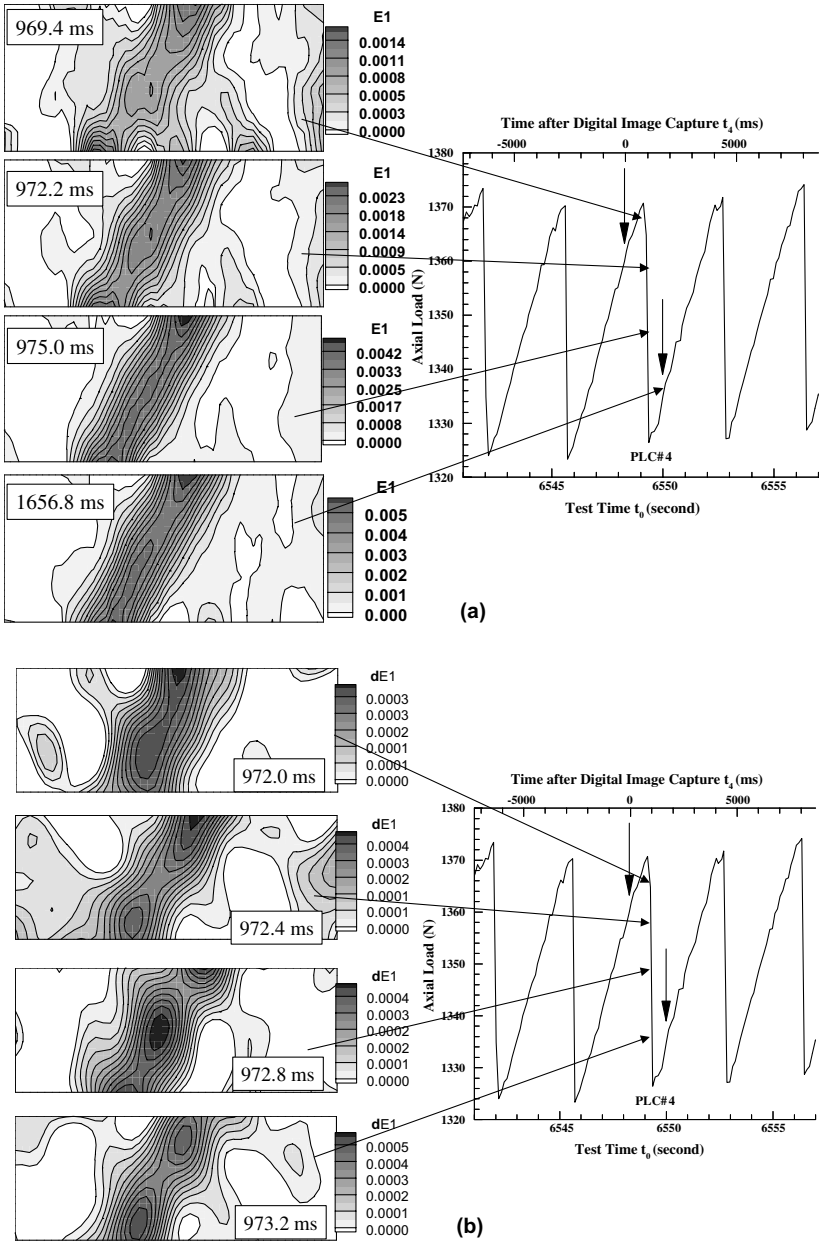

Fig. 3. PLC band #4: cumulative E_1 (a) and incremental dE_1 (b) axial strain maps (with a 9 mm × 4.6 mm field of view) at selected times. The time used here is t_4 with origin defined as the start of high-speed image captures shown in Fig. 2(a).

very high magnitude of the strain rate inside the band is not simply dictated by the compatibility condition of the imposed overall strain rate as $\frac{w_B}{2L_e}\frac{\dot{\varepsilon}_B}{\dot{\varepsilon}_a} \approx 460$–$920$ (where the band width at half height is $w_B/2 \approx 1.85$ mm and the total gage length of the sample $L_e \approx 20$ mm)!

The time history of cumulative axial strain at the center of PLC band #4 is shown in Fig. 4. Up to 80% or more of the total axial strain in the band was accumulated within a short period of 3–5 ms (accompanied by a sudden load drop of 2–4% of the current axial load level). Fig. 5 shows the time evolution of the axial strain distributions for PLC band #4 along the centerline of the tensile coupon around the location of each band. After initiation, PLC band #4 grew in a self-similar manner in terms of the spatial distribution of axial strain. In other words, the spatial distributions of axial strain at various times after band nucleation closely resemble one another if normalized by the corresponding peak strain level). No axial motion of the peak strain locations was observed (within the resolution of subpixel or a few microns) and the band width at half of the peak strain (i.e., the full width at the half magnitude) was found to be nearly constant (about 1.85 mm) throughout the rapid growth of the bands.

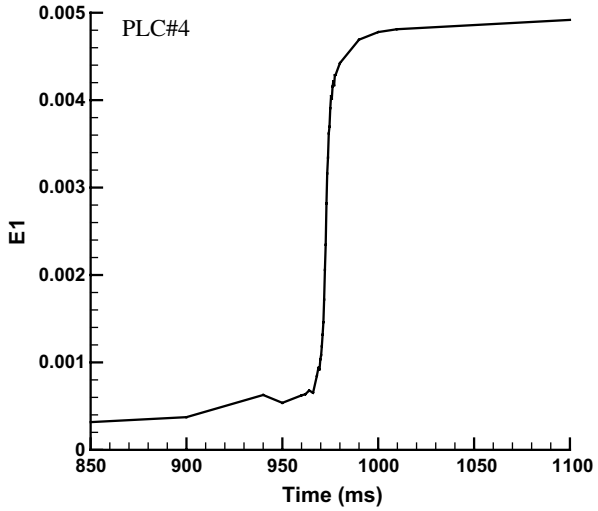

Fig. 4. The time history of the cumulative axial true strain at the center point of PLC band #4.

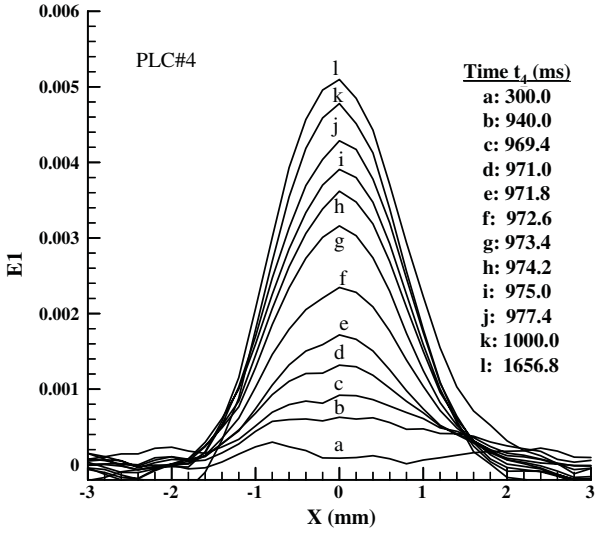

Fig. 5. True axial strain distributions of PLC band #4 along the centerline of the tensile coupon at selected times. The curves are plotted so that the peak strain in each band occurs at $X = 0$.

4. Discussion

At least two possible PLC band nucleation and subsequent development mechanisms in tensile test coupons have been proposed in the literature [3,25]. The first mechanism is associated with the initiation of an embryo band at a lateral specimen surface with subsequent transversal growth into the bulk at an angle (consistent with the resulting band orientation) with respect to the tensile axis. Such a band may have its final width and peak strain level at nucleation, and subsequently grows along its length direction to develop a complete band. The second mechanism is associated with nucleation and growth of a sample-scale band across the width and thickness of the tensile coupon but only a few atomic planes thick. This narrow band then expands in its width direction (along the specimen axis) until its expansion is blocked by the stress relaxation. Chihab et al. [3] associated these two scenarios of band development with different types of PLC bands observed in their experiments. For example, type C bands were thought to be related to the first mechanism, and types A and B bands largely result from the second mechanism. However, Chihab et al. [3] could not verify their hypotheses due to the lack of direct strain measurements and the very limited time resolution (25 fps) in their experiments. The PLC bands observed in our investigation fall into the type B bands according to the definition by Chihab et al. [3]. Some strain concentrations were indeed found to start to accumulate (prior to any obvious serrations or sudden load drops in the load–time curve) at one of the edges of the tensile coupon according to our time-resolved direct strain measurement results. However, the PLC bands were not first fully developed at a tensile coupon edge to their peak strain levels of 0.6%. Neither did fully developed strain concentrations of such a magnitude subsequently propagate within 3–5 ms along their length directions to form complete bands across the specimen width at the angle of ±26° with respect to the transverse direction (the representative PLC band #4 described in details here had an angle of −26°). As shown in incremental strain maps of Fig. 3(b), the material along the entire band region participated in plastic deformation throughout the entire 3–5 ms duration of the sudden load drops although some strain heterogeneities during the band growth was also evident.

Our strain measurement results did not show any significant expansion of type B PLC bands along the width direction of the bands (the tensile loading direction) during their growth. This is clearly confirmed by the axial strain distribution profiles shown in Fig. 5. As the strain profiles remained self-similar, no major motion of the band strain distributions (either cumulative or incremental) along the tensile loading direction occurred within the 3–5 ms of the band development period. Contrary to the usual assumption of a uniform band strain distribution with step-like transitions (which is consistent with the second mechanism proposed by Chihab et al. [3]), our strain measurement results show that the PLC bands have a more or less symmetric but bell-like strain distribution throughout the entire 3–5 ms nucleation and development period. Such strain distribution characteristics are similar to those observed in localized necks in sheet metals due to material tension instability at large strains [26].

At the time resolution of 0.2 ms and the spatial resolution of the average grain size, the type B PLC bands studied here appear to be purely stationary at the macroscopic level as no plastic deformation front was

detected to propagate either along the band's length direction or along the band's width direction (the tensile loading direction). This is clearly demonstrated by the incremental maps in Fig. 3(b): the successive "snapshots" of the each band suggest no transverse or lateral motion of the deformation fronts of any kind. In summary, PLC bands of the type B are more or less just a series of discrete, localized necks with a certain peak strain and a characteristic bell-like strain profile.

Acknowledgement

The high-speed digital image acquisition was carried out with the help of Mr. Andy Kubit of Vision Research (Wayne, NJ) and the AA 5052-H32 sheet metal material was provided by Dr. Tim Focke of NIST (Gaithersburg, MD). The enthusiastic support of Drs. Alan Taub, Shawn Gayden, and Y.T. Cheng and the critical review of Dr. Paul E. Krajewski of the manuscript are gratefully acknowledged.

References

[1] Cottrell AH. Dislocations and plastic flow in crystals. Oxford: Clarendon Press; 1953.
[2] Hall EO. Yield point phenomena in metals and alloys. London: Macmillan; 1970.
[3] Chihab K, Estrin Y, Kubin LP, Vergnol J. Scripta Metall 1987; 21:203.
[4] Kubin LP, Fressengeas C, Ananthakrishna G. Collective behavior of dislocations in plasticity. In: Nabarro FNN, Hirth JP, editors. Dislocation in solids, vol. 11. New York: Elsevier Science; 2001.
[5] McCormick PG, Venkadesan P, Ling CP. Scripta Metall Mater 1993;29:1159.
[6] Weinhandl H, Mitter F, Bernt W, Kumar S, Pink E. Scripta Metall Mater 1994;31:1567.
[7] Wack B, Tourabi A. Mater Sci Eng A 1995;196:79.
[8] Fujita H, Tabata T. Acta Metall 1977;25:793.
[9] Korbel A, Zasadzinski J, Sieklucka Z. Acta Metall 1976;24: 919.
[10] Robinson JM. Int Mater Rev 1994;39:217.
[11] Gallardo-Lopez A, Gomez-Garcia D, Dominguez-Rodriguez A, Kubin LP. Scripta Mater 2004;51:203.
[12] Nagarjuna S, Anozie FN, Evans JT. Mater Sci Tech 2003;19: 1661.
[13] Zhu SM, Gao X, Nie JF. In: Luo A, editor. Magnesium technology 2004. Warrendale, PA: The Minerals, Metals & Materials Society; 2004. p. 325.
[14] Cheng XM, Morris JG. Scripta Mater 2000;43:651.
[15] Lebyodkin M, Brechet Y, Estrin Y, Kubin LP. Key Eng Mater 1995;103:313.
[16] Mesarovic S. J Mech Phys Solids 1995;43:671.
[17] Bruck HA, McNeill SR, Sutton MA, Peters WH. Exp Mech 1989; 29:261.
[18] Chen DJ, Chiang FP, Tan YS, Don HS. Appl Optics 1993;32: 1839.
[19] Tong W. Exp Mech 1997;37:452.
[20] Vendroux G, Knauss WG. Exp Mech 1998;38:86.
[21] Tong W. J Mech Phys Solids 1998;46:2087.
[22] Staley JT. Effects of composition, processing and structure on aluminum alloys. In: Materials selection and design. ASM metals handbook, 20. OH: Materials Park; 1985.
[23] Phantom V9.0, Vision Research, http://www.visiblesolutions.com.
[24] Tong W. A User's Guide to the Yale Surface Deformation Mapping Program (SDMAP), Technical Report, Department of Mechanical Engineering, Yale University, New Haven, CT (1996–2004).
[25] Kocks UF. In: Progress in materials science. Chalmers anniversary volume. Oxford: Pergamon Press; 1981. p. 225.
[26] Tong W, Zhang N. Proceedings of the ASME manufacturing engineering division MED, vol.12. New York: ASME; 2001.